Element-quality-based stiffening for the pseudoelastic mesh-moving technique

Element-quality-based stiffening for the pseudoelastic mesh-moving technique

D. Ishihara*, A. Goto, M. Onishi, T. Horie, T. Niho

Department of Mechanical Systems Engineering, Kyushu Institute of Technology, 680-4 Kawazu, Iizuka, Fukuoka 820-8502, Japan

SUMMARY

In this study, element-quality-based stiffening (EQBS) was developed as a method of maintaining mesh quality in the pseudoelastic mesh-moving technique. The proposed EQBS technique increases the stiffness of the element based on two element quality parameters, the element area and shape; this differs from techniques used in previous studies. Importantly, EQBS includes the previously proposed Jacobian-based stiffening (JBS) and minimum height-based stiffening (MHBS) techniques as a specific case. Therefore, it is quite general scenario of the selective stiffening of the mesh. The proposed EQBS technique was applied to the mesh-moving of a rectangular domain including a structure consisting of a square and a fin that undergo large translations and rotations. The proposed EQBS technique showed better performance than JBS on test problems with large translations and rotations applied to the structure. This is because EQBS considers the shear deformation of the element in addition to the tensile and compressive deformations.

KEY WORDS: Pseudoelastic mesh-moving technique; Interface tracking method; Fluid–structure interactions; Finite element method

1. INTRODUCTION

Fluid–structure interaction (FSI) analysis poses a great challenge in scientific and engineering problems considering complex geometries, high nonlinearity, and strong instabilities, including problems considering structures undergoing large translations and rotations [1–3]. Interface-tracking methods, such as the arbitrary Lagrangian–Eulerian (ALE) method [4–7] and the deforming-spatial-domain/stabilized space–time (DSD/SST) method [8], are suitable for such FSI problems, for which moving interfaces should be described accurately. Mesh updating is required in these methods, and the mesh must be updated and deform to follow the motion of the interface. Mesh updating methods can be roughly classified into the mesh-moving and remeshing methods.

In the mesh-moving method, the nodes are moved according to the motion of the interface while maintaining the connectivity of the nodes. Therefore, the excessive motion of the interface may decrease the mesh quality. In contrast, remeshing requires automatic mesh generation, which is a very computationally expensive process. Furthermore, the projection of the solution from the old mesh to the new one tends to introduce numerical error. Therefore, it is reasonable to use mesh updating based on a combination of the mesh-moving method and partial remeshing for the excessive element distortion [17], which allows the mesh quality in the mesh-moving technique to be maintained.

The mesh-moving techniques developed and implemented in previous studies can be classified as follows [20]:

- Interpolated deformations [9, 10]
- Laplacian approaches [11, 12]
- Discrete spring methods [13–16]
- Pseudoelastic analogy [17–19].

In the pseudoelastic mesh-moving technique, the fluid mesh is modeled as a pseudoelastic mesh, and finite element linear elastic analysis is performed using the displacement on the moving boundary as the elementary boundary condition. The resulting nodal displacement is used to

move the corresponding node. This type of method has been gaining popularity because of the generality of the finite element method. Therefore, the pseudoelastic mesh-moving technique was used in this study.

In the pseudoelastic mesh-moving technique, the selective stiffening of the mesh is used to maintain the mesh quality. One of the pioneer works on the selective stiffening of the mesh was the development of Jacobian-based stiffening (JBS) [17], in which the stiffness of the element increases as its area decreases. More recently, minimum height-based stiffening (MHBS) [19] has been proposed. In this method, the stiffness of the element increases as its minimum height decreases.

As seen in the effort of these studies, the pseudoelastic mesh-moving technique always requires the selective stiffening that can give the higher mesh quality. Therefore, the purpose of this study is to develop a new stiffening method to give the higher mesh quality.

In this paper, element-quality-based stiffening (EQBS) is proposed. In the proposed EQBS technique, the stiffness of the element increases based on both the area and aspect ratio of the element. Importantly, the proposed EQBS technique includes JBS and MHBS as specific cases. Therefore, it is quite general scenario of the selective stiffening of the mesh.

JBS evaluates only the area of each element. On the contrary, the proposed EQBS uses the weighted evaluation for both the area and the aspect ratio of each element. From the viewpoint of EQBS, MHBS can be understood as the method using the equally weighted evaluation for both the area and the aspect ratio of each element.

JBS does not change the evaluation in the element, where the aspect ratio increases while the area is constant. Of course, JBS decreases the quality of this element. The shear deformation does not contribute to the area change. Therefore, JBS will be weak for the shear deformation. On the contrary, the proposed EQBS will be adaptive for the shear deformation, since it can change the weighted evaluation for both the area and the aspect ratio of each element as the magnitude of the shear deformation changes, while

MHBS cannot changes this weighted evaluation.

The superior ability of EQBS to maintain the mesh quality in comparison to that of JBS and MHBS was demonstrated by applying the mesh-moving technique to a rectangular domain containing a structure consisting of a square and a fin that underwent large translations and rotations. This test problem has geometric and kinematic characteristics similar to those of the FSI problem of insect flapping flight [2, 3, 21, 22]. Therefore, the proposed EQBS technique will be applied to this FSI problem in future works.

The fin was used in the previous studies [17][19]. Similar to these studies, the fin translates and rotates with the large magnitude. Note that the maximum magnitude in this study is larger than that in the previous studies. Therefore, the present problem corresponds to that used in the previous studies. In addition, the present structure also includes the bluff body as well as the fin. This type of the structure can be found in the benchmark problems [23-26] as well as the flexible elastic wings [2, 3, 22]. In this study, because of these similarity and generality, the present test problem is used.

As shown in the present results, the proposed EQBS can give the higher mesh quality adaptively using the various selections of the control parameters including JBS and MHBS. It follows that the proposed EQBS is the robust selective stiffening of the mesh to give the higher mesh quality.

2. PSEUDOELASTIC MESH-MOVING TECHNIQUE

2.1. Governing equation of the pseudoelastic domain

Let us consider Ω as the spatial domain and Γ as its boundary. Γ consists of the boundary Γ_u with the essential boundary condition and the boundary Γ_τ with the natural boundary condition. In the pseudoelastic mesh-moving technique, a pseudoelastic mesh occupies Ω, and its displacement along the moving boundary is imposed on Γ_u. The equilibrium equation for the elastic body is considered to be the governing equation for the pseudoelastic material, which can be expressed as

$$\frac{\partial \sigma_{ji}}{\partial x_j} + f_i = 0 \quad \text{in } \Omega, \tag{1}$$

where σ_{ij} is the ijth component of the Cauchy stress tensor and f_i is the ith component of the external force vector. Hooke's law was used to describe the relationship between σ_{ij} and the strain tensor ε_{ij}, where ε_{ij} is defined as

$$\varepsilon_{ij} = \frac{1}{2}\left(\frac{\partial u_i}{\partial x_j} + \frac{\partial u_j}{\partial x_i}\right). \tag{2}$$

The essential and natural boundary conditions are respectively given as

$$u_i = \bar{u}_i \text{ on } \Gamma_u \quad \text{and} \quad \sigma_{ij} n_j = \tau_i \text{ on } \Gamma_\tau, \tag{3a, b}$$

where $\bar{u}_i$ is the displacement prescribed on Γ_u and τ_i is the traction force acting on Γ_τ.

2.2. Space discretization

Applying the finite element formulation to the governing equation given by Eq. (1), the discrete equation system can be obtained in matrix form as

$$\left(\sum_{e}[\mathbf{K}_e]\right)\{\mathbf{u}\}=\mathbf{0} \quad \text{and} \quad \mathbf{K}_e=\int_{\Xi}[\cdots]_e J_e \mathrm{d}\Xi, \tag{4a, b}$$

where **K** is the stiffness matrix, the subscript e denotes the elemental quantity, **u** is the nodal displacement vector for the pseudoelastic mesh, […] represents the terms being integrated, and Ξ is the parent domain. The Jacobian J_e for element e is defined as

$$J_e=\det\left(\frac{\partial \mathbf{x}}{\partial \boldsymbol{\xi}}\right), \tag{5}$$

where **x** and **ξ** represent the global and local coordinates, respectively. In this study, no external forcing function was defined to selectively handle mesh motion, and the external force vector was thus set to **0**.

2.3. Formulation using the stiffening coefficient

In the pseudoelastic mesh-moving technique, the stiffness matrix given in Eq. (4b) is redefined as

$$\mathbf{K}_e \mapsto \int_{\Xi}\kappa_e[\cdots]_e J_e \mathrm{d}\Xi, \tag{6}$$

where κ_e is the stiffening coefficient for each element. κ_e is used to control the stiffness of each element and selectively handle mesh motion.

In a previous studies, κ_e was given as follows:

- Jacobian–based stiffening (JBS) [17]

$$\kappa_e=\left(\frac{J_0}{J_e}\right)^{\chi}, \tag{7a}$$

where χ is the stiffening power, which must be nonnegative, and J_0 is an arbitrary scaling parameter inserted into the formula to ensure dimensional consistency.

- Minimum–height–based stiffening (MHBS) [19]

$$\kappa_e = \left(\frac{h_0}{h_e^{\min}} \right)^{\chi}, \tag{7b}$$

where $h_e^{\min}$ is the minimum height for element e, and h_0 is an arbitrary scaling parameter.

In this study, a linearly interpolated triangular element was used. In this case, the linear equation system for the pseudoelastic mesh-moving technique can be written as

$$\left(\sum_e \kappa_e [\mathbf{K}_e] \right) \{\mathbf{u}\} = \mathbf{0}, \tag{8}$$

and Eq. (7a) can be reduced to

$$\kappa_e = \left(\frac{A_0}{A_e} \right)^{\chi}, \tag{9}$$

where A_e is the area of element e, and A_0 is the scaling parameter with the dimension of area.

3. ELEMENT-QUALITY-BASED STIFFENING

The mesh quality can be evaluated using the following measures [17]:

$$\max_e f_e^{\mathrm{A}} \quad \text{and} \quad \max_e f_e^{\mathrm{R}}, \tag{10a, b}$$

where f_e^{A} and f_e^{R} are the changes in the area and shape of the element, respectively. They are defined as

$$f_e^{\mathrm{A}} = \left| \log\left(\frac{A_e}{A_e^{\mathrm{o}}} \right) \right| \tag{11a}$$

and

$$f_e^{\mathrm{R}} = \left| \log\left(\frac{R_e}{R_e^{\mathrm{o}}} \right) \right|, \tag{11b}$$

where A_e and R_e are the area and aspect ratio of element e, respectively, and the superscript o refers to the undeformed mesh. R_e is defined as

$$R_e = \frac{\left(l_e^{\max}\right)^2}{A_e} = \frac{l_e^{\max}}{h_e^{\min}}, \tag{12}$$

where $l_e^{\max}$ is the maximum edge for element e, and the relation of A_e equal to the multiplication of $l_e^{\max}$ and $h_e^{\min}$ is used in the last expression.

It follows from these equations that A_e and R_e are the fundamental parameters in the mesh quality measures. Therefore, the stiffening coefficient κ_e can use these two parameters to maintain the mesh quality. On this basis, a definition of the stiffening coefficient κ_e that includes the element quality is proposed as

$$\kappa_e = \left(\left(\frac{A_0}{A_e} \right)^{\chi_1} R_e^{\chi_2} \right)^{\chi_3}, \tag{13}$$

where χ_1 and χ_2 satisfy the relationship $\chi_1 + \chi_2 = 1.0$ because they define the weights of the element quality parameters A_e and R_e. The use of this coefficient constitutes the EQBS technique. Note that EQBS can be extended to three-dimensional mesh using V_e as A_e and $A_e^{\max}$ as $l_e^{\max}$ in Eqs.(12) and (13), where V_e and $A_e^{\max}$ are the volume and the maximum surface for element e, and $h_e^{\min}$ is given as V_e divided by $A_e^{\max}$.

Importantly, EQBS reduces to JBS for $\chi_1 = 1.0$ and $\chi_2 = 0.0$, and MHBS for $\chi_1 = \chi_2 = 0.5$, as shown by substituting these values into Eq. (13):
$\chi_1 = 1$ and $\chi_2 = 0$ reduces Eq. (13) to

$$\kappa_e = \left(\frac{A_0}{A_e} \right)^{\chi_3}, \tag{14a}$$

which is equivalent to Eq. (9). Similarly, $\chi_1 = \chi_2 = 0.5$ reduces Eq. (13) to

$$\kappa_e = \left(\left(\frac{A_0}{A_e} \right)^{0.5} R_e^{0.5} \right)^{\chi_3} = \left(\frac{A_0^{0.5}}{h_e^{\min}} \right)^{\chi_3}, \tag{14b}$$

where Eq. (12) is used to obtain the last expression. The last expression of Eq. (14b) gives the coefficient equivalent to Eq. (7b). Therefore, the proposed EQBS is the quite general scenario and includes both JBS and MHBS as a specific case.

4. NUMERICAL EXAMPLES

4.1. Problem setup

A rectangular domain including a rigid body consisting of a square and a fin was considered, as shown in Figure 1. Point O is located on the base of the square, and point A is located on the tip of the fin. A Cartesian coordinate system was used with the origin coinciding with point O. Roller supports were imposed along the outer boundary of the rectangular domain, as shown in Figure 1. In the case of translation, a translational displacement u_x in the x-direction was applied to the rigid body. In the case of rotation, a rotational displacement θ_z about the z-axis was applied to the rigid body. This problem has geometric and kinematic characteristics similar to those of the FSI problem of insect flapping flight [2, 3, 21, 22].

4.2. Analysis setup

As shown in Figure 2 (a), the incremental displacement Δu is defined as u_x/N or θ_z/N, where N is the total number of incremental steps. In the actual analysis, N corresponds to the number of time steps for one cycle of the period. χ_1, χ_2, χ_3, and N were determined using the prescribed reference displacement, which is denoted by $u_x^{(0)}$ or $\theta_z^{(0)}$, as follows.

Step 1

Figure 2 (b) shows the flow of this step schematically. JBS (EQBS with (χ_1, χ_2) = (1.0, 0.0)) with a typical parameter value of χ_3 = 2.0 [17] was considered, and N was set to a positive integer. N was then updated such that the changes in the mesh quality measures (Eqs. (10a) and (10b)) over the whole domain remained less than 5% as N increased.

Step 2

Figure 2 (c) shows the flow of this step schematically. χ_1 was set to values ranging from 0.0 to 1.0 in increments of 0.1, and χ_2 was calculated as $1 - \chi_1$. Then, χ_3 was obtained with an accuracy of 0.1 as the value that minimizes the mesh quality measure of Eq. (10b) over the whole domain.

The following sections discuss the mesh deformation test cases performed in this study for a two-dimensional (2D) mesh consisting of

linearly interpolated triangular elements around the rigid body, as shown in Figure 3. The rigid body consists of a square and a fin, and the thickness of the fin was set to zero. The number of nodes and elements were 4,641 and 8,996, respectively.

4.3. Large translation

The reference value $u_x^{(0)}$ was set to 10 cm, and N was determined to be 15 using the procedure outlined in Step 1 of Section 4.2.

Then, χ_3 was determined for the prescribed sets of χ_1 and χ_2 using the procedure given in Step 2 of Section 4.2; the results are given in Table 1.

Figures 4 and 5 show the changes in the mesh quality measures (Eqs. (10a) and (10b)) plotted against the translation u_x. The mesh qualities were measured in the domain near the structure, as shown in Figure 3(b). As shown in Figures 4 and 5, EQBS with $(\chi_1, \chi_2) = (0.5, 0.5)$ or MHBS showed the best performance in terms of maintaining the mesh quality under large translational deformations. Similarly, EQBS with $(\chi_1, \chi_2) = (0.6, 0.4)$ and $(0.4, 0.6)$ performed second best under large deformations. On the basis of this observation, it was concluded that EQBS with $\chi_1 \approx \chi_2$ shows the best performance in terms of the maintenance of the mesh quality under a large translational deformation.

Figures 6 and 7 show the moved meshes under the maximum considered translation of $u_x = 30$ cm, where the color contours of the tensile/compressive strain in the x-direction ε_{xx}, and the shear strain ε_{xy} the strain fields are drawn. As shown in Figure 6, $u_x = 30$ cm is a large translation that spans approximately 80% of the x-distance between the original position of the rigid body and the domain boundary. The translation of the rigid body produces a shear stress in the vicinities of the sharp corners of the square and the tip of the fin.

Let us recall that JBS uses a stiffness coefficient that includes only the element area. JBS does not change the evaluation for the element that increases the aspect ratio while keeps the area constant. The shear deformation does not contribute to the area change. Therefore, JBS will be weak for the shear deformation. JBS produces the significant transition of ε_{xx} with the change of the sign as shown in Figure 7 (a), or large ε_{xy} as shown in Figure 8 (a) because of the stress concentration in the vicinity of

the lower end of the fin. On the contrary, as shown in Figures 7(b) and 8(b), EQBS with $\chi_1 \approx \chi_2$ such as MHBS limits mesh distortion resulting from the shear deformation because it takes into account the element shape as well as the element area with weights of χ_1 and χ_2, respectively.

4.4. Large rotation

The reference value $\theta_z^{(0)}$ was set to 30°, and N was determined to be 15 using the procedure outlined in Section 4.2. χ_3 was then determined for the prescribed set of χ_1 and χ_2 using the procedure in Section 4.2, and the results are given in Table 2.

Figures 9–12 show the changes in the mesh quality measures (Eqs. (10a) and (10b)) plotted against the rotation θ_z. The mesh qualities were measured in the domain near the structure, as shown in Figure 3(b). The ability of the proposed EQBS technique to maintain the element area did not differ greatly from that of JBS, as shown in Figure 9; however, EQBS with $(\chi_1, \chi_2) = (0.3, 0.7)$ showed the best performance among the stiffening techniques with different parameters for rotations larger than about 120°, as shown in Figure 10. Furthermore, for rotations smaller than approximately 60°, the ability of EQBS to maintain the element shape did not differ greatly from that of JBS, as shown in Figure 11, and EQBS with $(\chi_1, \chi_2) = (0.3, 0.7)$ showed the best performance among the EQBS techniques with different parameters for rotations larger than approximately 60°, as shown in Figure 12. From this observation, EQBS with $\chi_1 < \chi_2$ shows better performance than stiffening with different parameter values in terms of maintaining the mesh quality under large rotations.

Figures 13, 14, and 15 show the moved meshes for a maximum rotation of $\theta_z = 150°$, where the color contours of the tensile/compressive strain in the x-direction ε_{xx}, and the shear strain ε_{xy} the strain fields are drawn. As shown in Figure 13, the mesh became twisted around the structure after the rotation. This type of motion induced a large shear stress in the vicinity of the structure.

The proposed EQBS will be adaptive for the shear deformation, since it can change the weighted evaluation for the area and the aspect ratio of each element as the magnitude of the shear deformation changes. On the contrary, JBS uses only the evaluation for the area, and MHBS uses only

the equally weighted evaluation for the area and the aspect ratio irrespective of the change of the magnitude of the shear deformation. Therefore, the mesh quality from the proposed EQBS with $\chi_1 < \chi_2$ was higher than those from JBS and MHBS as the structural rotation increases or the shear deformation surrounding the structure increases. JBS produces the significant transition of ε_{yy} with the change of the sign from the lower end of the fin to the corner of the square body as shown in Figure 14 (a), or large ε_{xy} as shown in Figure 15 (a). On the contrary, EQBS reduces this shear deformation. Especially, EQBS with $(\chi_1, \chi_2) = (0.3, 0.7)$ clearly reduces this shear deformation as shown in Figures 14 (c) and 15 (c).

5. CONCLUDING REMARKS

In this study, the stiffening coefficient used in the pseudoelastic mesh-moving technique was redefined for application in EQBS, a technique that can be used to maintain the mesh quality. The proposed EQBS technique is based on two element quality parameters, the element area and shape, which are in a tradeoff relationship. Their weights and the stiffening effect were determined using these two parameters and a third independent parameter. Importantly, EQBS includes both JBS and MHBS, which were proposed in previous studies, as a specific case. To demonstrate the performance of EQBS, it was applied to the mesh-moving of a rectangular domain including a structure consisting of a square and a fin undergoing large translations and rotations.

For large translations, EQBS with equivalent weights for the element area and shape or MHBS show better performance than JBS did. This is because large translations of the structure produce large shear deformations in addition to the tensile and compressive deformations of the mesh in the vicinity of the structure. For large rotations, EQBS with the weight for the element shape exceeding that for the element area showed better performance than EQBS with any other weight combination. This is because large rotations of the structure produce large shear deformations in the mesh elements in the vicinity of the structure.

It follows that the proposed EQBS always gives the mesh quality higher than or equal to that given by JBS and EQBS. In future work, the proposed EQBS technique will be applied to the FSI problem of insect flapping flight. In this problem, a flexible and thin wing with a stiff, thick leading edge sweeps the air with a large translation and rotation; the geometric and kinematic characteristics of this problem are very similar to those of the present test problem.

ACKNOWLEDGEMENTS

This work was supported by JSPS KAKENHI Grant Number 17H02830.

REFERENCES

1. Takizawa K, Tezduyar TE. Computational methods for parachute fluid-structure interactions. *Archives of Computational Methods in Engineering* 2012; 19:125-169.
2. Nakata T, Liu H. A fluid-structure interaction model of insect flight with flexible wings. *Journal of Computational Physics* 2012; 231:1822-1847.
3. Ishihara, D, Horie T, Niho T. An experimental and three-dimensional computational study on the aerodynamic contribution to the passive pitching motion of flapping wings in hovering flies. *Bioinspiration & Biomimetics* 2014; 9:046009 (23pp).
4. Hirt CW, Amsden AA, Cook JL. An arbitrary Lagrangian–Eulerian computing method for all flow speeds. *Journal of Computational Physics* 1974; 14:227–253.
5. Hughes TJR, Liu WK, Zimmerman TK. Lagrangian–Eulerian finite element formulation for incompressible viscous flows. *Computer Methods in Applied Mechanics and Engineering* 1981; 29:329–349.
6. Huerta A, Liu WK. Viscous flow with large free surface motion. *Computer Methods in Applied Mechanics and Engineering* 1988; 69:277–324.
7. Demirdzic I, Peric M. Space conservation law in finite volume calculations of fluid flow. *International Journal for Numerical Methods in Fluids* 1988; 8:1037–1050.
8. Tezduyar TE, Behr M, Liou J. A new strategy for finite element computations involving moving boundaries and interfaces–the deforming-spatial-domain/space–time procedure: I. The concept and the preliminary tests. *Computer Methods in Applied Mechanics and Engineering* 1992; 94:339–351.
9. Nomura T, Hughes TJR. An arbitrary Lagrangian–Eulerian finite element method for interaction of fluid and a rigid body. *Computer Methods in Applied Mechanics and Engineering* 1992; 95:115 –138.
10. Lefrancois E. Numerical validation of a stability model for a flexible over-expanded rocket nozzle. *International Journal for Numerical Methods in Fluids* 2005; 49(4):349–369.

11. Zhang Q, Hisada T. Analysis of fluid-structure interaction problems with structural buckling and large domain changes by ALE finite element method. *Computer Methods in Applied Mechanics and Engineering* 2001;190:6341– 6357.
12. Helenbrook BT. Mesh deformation using the biharmonic operator. *International Journal for Numerical Methods in Engineering* 2003; 56:1007–1021.
13. Batina JT. Unsteady Euler algorithm with unstructured dynamic mesh for complex-aircraft aeroelastic analysis. *AIAA-89-1189*, 1989.
14. Degand C, Farhat C. A three-dimensional torsional spring analogy method for unstructured dynamic meshes. *Computers and Structures* 2002; 80:305–316.
15. Bottasso CL, Detomi D, Serra R. The ball-vertex method: a new simple spring analogy method for unstructured dynamic meshes. *Computer Methods in Applied Mechanics and Engineering* 2005; 194:4244–4264.
16. Blom FJ. Considerations on the spring analogy. *International Journal for Numerical Methods in Fluids* 2000; 32:647–668.
17. Stein L, Tezduyar T, Benney R. Automatic mesh update with the solid-extension mesh moving technique. *Computer Methods in Applied Mechanics and Engineering* 2004; 193:2019–2032.
18. Liu X, Qin N, Xia H. Fast dynamic grid deformation based on Delaunay graph mapping. *Journal of Computational Physics* 2006; 211:405–423.
19. Yamada T, Yamamoto Y, Hong G, Yoshimura S. A mesh moving technique with minimum–height–based stiffening for fluid-structure interaction analysis, *Mechanical Engineering Letters* 2017; 3:16-00657 (8 pages).
20. Lefrancois E. A simple mesh deformation technique for fluid–structure interaction based on a submesh approach, *International Journal for Numerical Methods in Engineering* 2008; 75:1085-1101.
21. Ishihara D, Horie T, Denda M. A two-dimensional computational study on the fluid-structure interaction cause of wing pitch changes in dipteran flapping flight, *The Journal of Experimental Biology* 2009; 212:1-10.
22. Ishihara D, Horie T. Passive mechanism of pitch recoil in flapping insect wings, *Bioinspiration & Biomimetics* 2017; 12:016008 (15

pages).
23. Wall WA, Ramm E. Fluid-structure interaction based upon a stabilized (ALE) finite element method, *Proceedings of the 4th World Congress on Computational Mechanics New Trends and Applications* 1998; CD-ROM, CIMNE.
24. Dettmer WG, Peric D. A computational framework for fluid-structure interaction: finite element formulation and applications. Computer Methods in Applied Mechanics and Engineering 2006; 195:5754-5779.
25. Yamada T, Yoshimura S. Line search partitioned approach for fluid-structure interaction analysis of flapping wing, *Computer Modeling in Engineering and Sciences* 2008; 24:51-60.
26. Matthies HG, Steindorf J. Partitioned strong coupling algorithms for fluid-structure interaction, Computers and Structures 2003; 81:805-812.

FIGURES

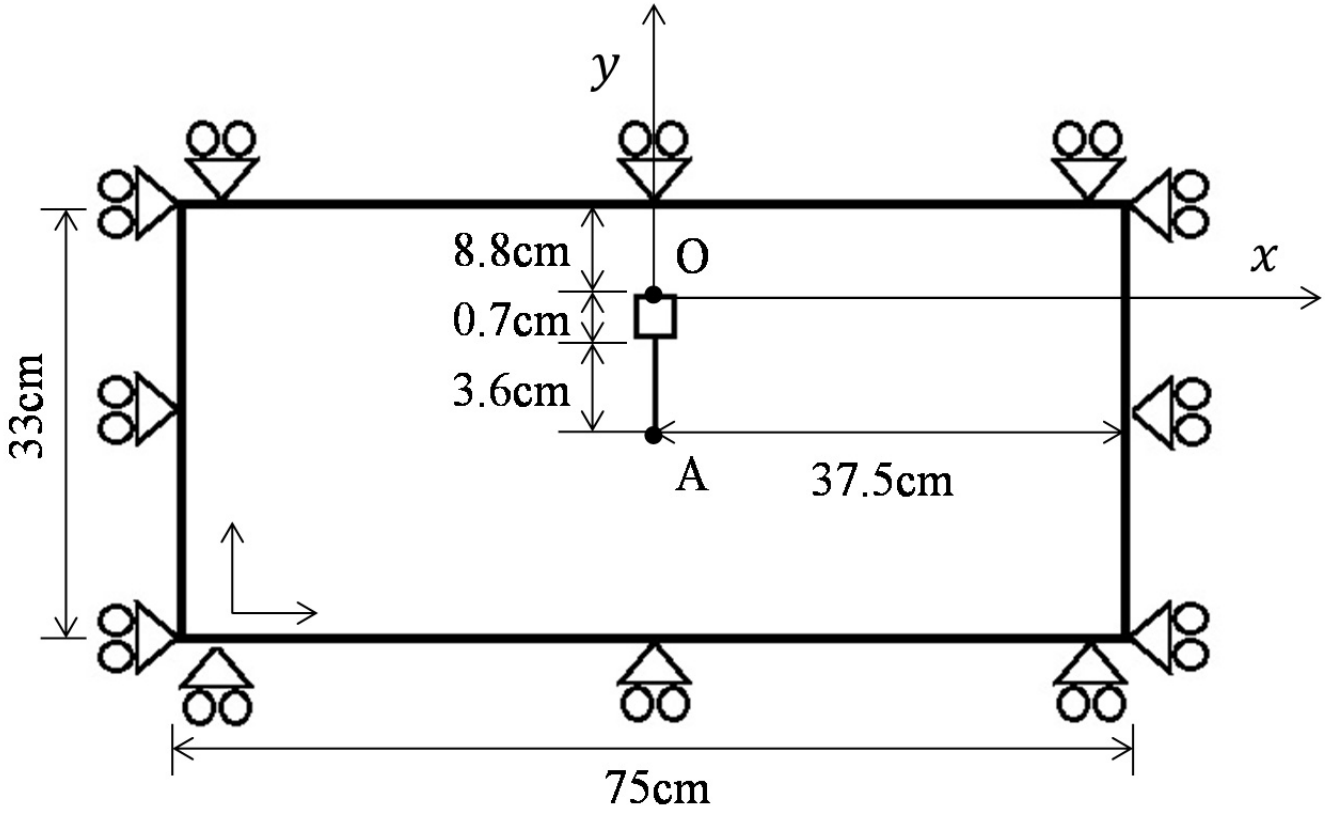

Figure 1 Schematic of the problem setup. The rectangular domain surrounding the structure was considered. The structure is rigid and consists of a square domain and a domain of zero thickness. The structure underwent large translations and rotations. The medium in the rectangular domain was assumed to be attached to the structure at the structure–medium interface. Therefore, the rectangular domain deforms to follow the motion of the structure. Roller supports were imposed along the outer boundary of the rectangular domain.

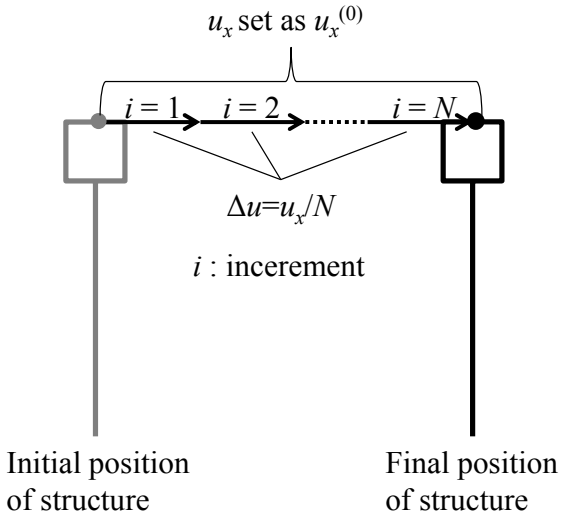

(a) Relation among $u_x = u_x^{(0)}$, Δu, and N

Step 1:
Find enough large N (see the above figure) using JBS or $(\chi_1, \chi_2) = (1.0, 0.0)$ as follows:

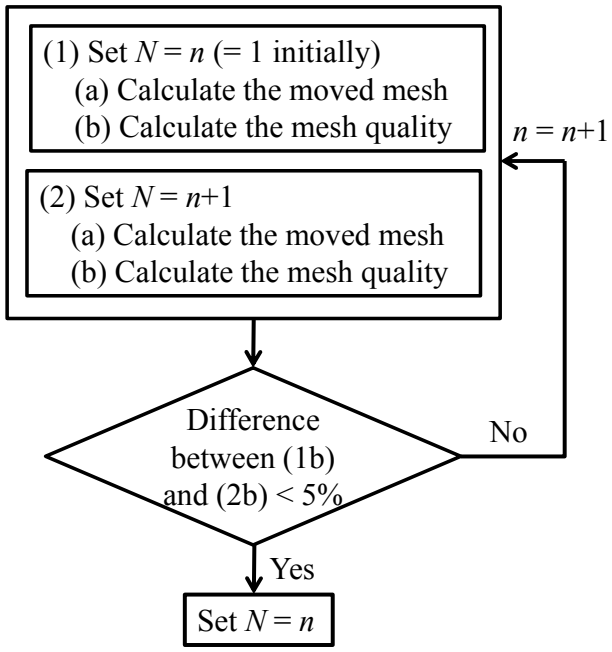

(b) Flow of Step 1

Step 2:
Find the best χ_3 for (χ_1, χ_2) as follows:

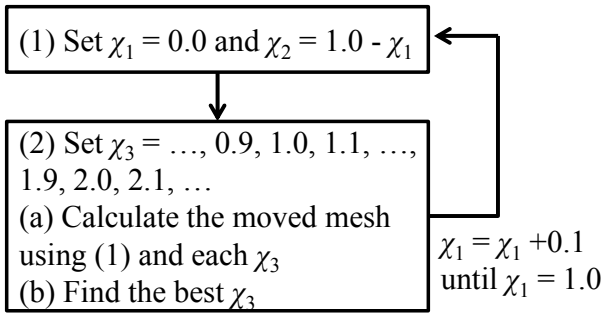

(b) Flow of Step 2

Figure 2 Flow to determine the parameters N, χ_1, χ_2, and χ_3 in this study.

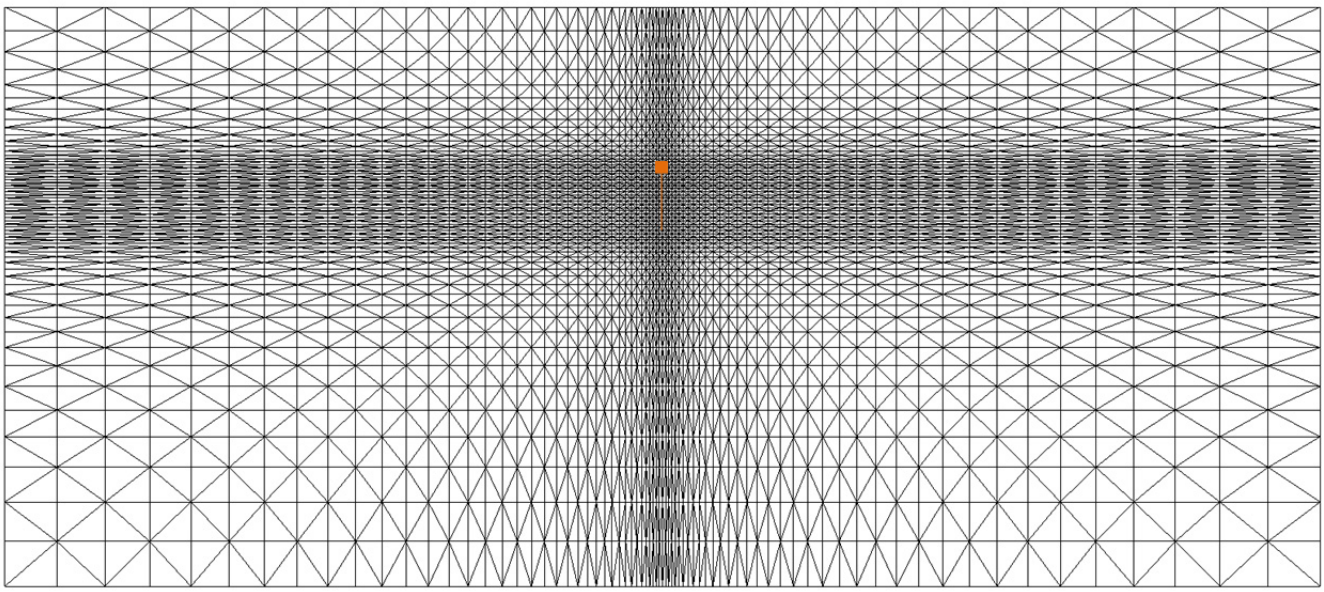

(a) Mesh in the entire domain

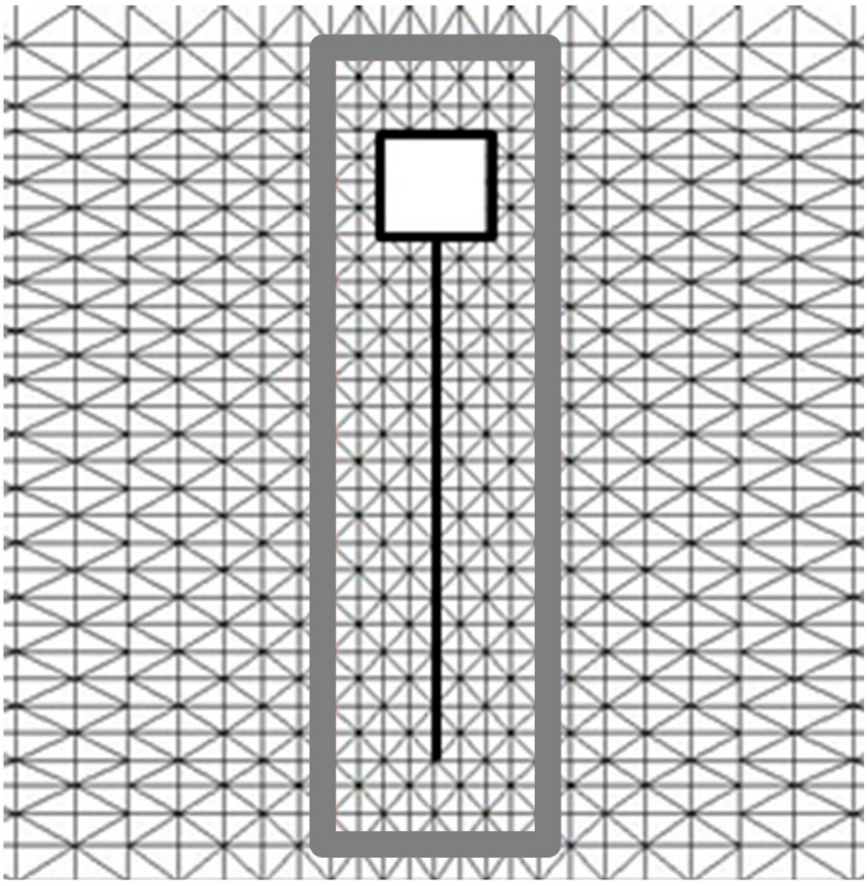

(b) Detail of the mesh near the structure

Figure 3 2D mesh composed of linearly interpolated triangular elements around the rigid body. The orange region in (a) is the rigid body. The mesh qualities of element shape and area were measured in the domain bounded by the gray bold line in (b) to demonstrate the performance of the EQBS and JBS techniques.

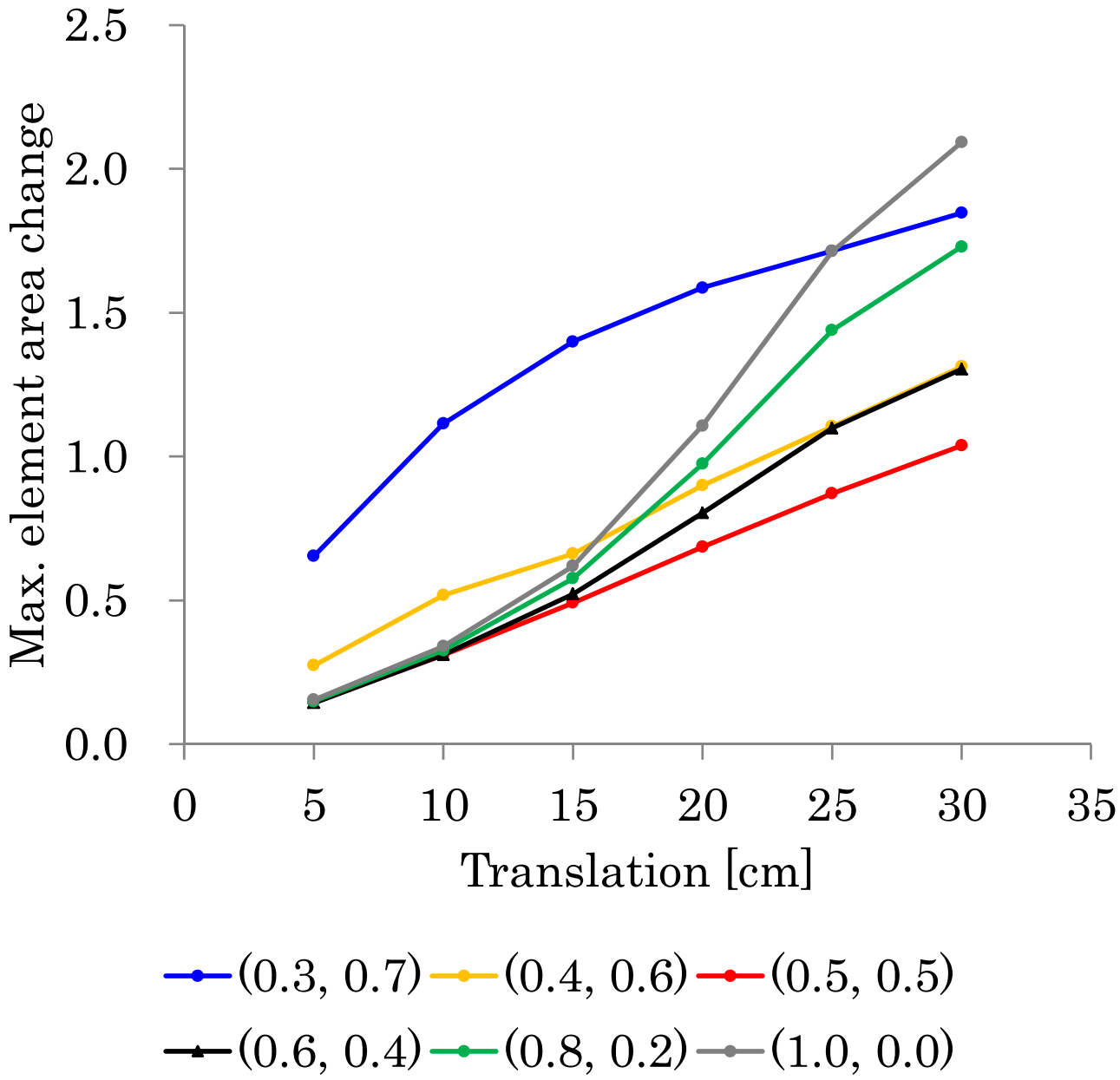

Figure 4 Maximum element area change plotted against the translation of the structure for EQBS with different (χ_1, χ_2) values. (χ_1, χ_2) = (1.0, 0.0) and (0.5, 0.5) correspond to JBS and MHBS, respectively.

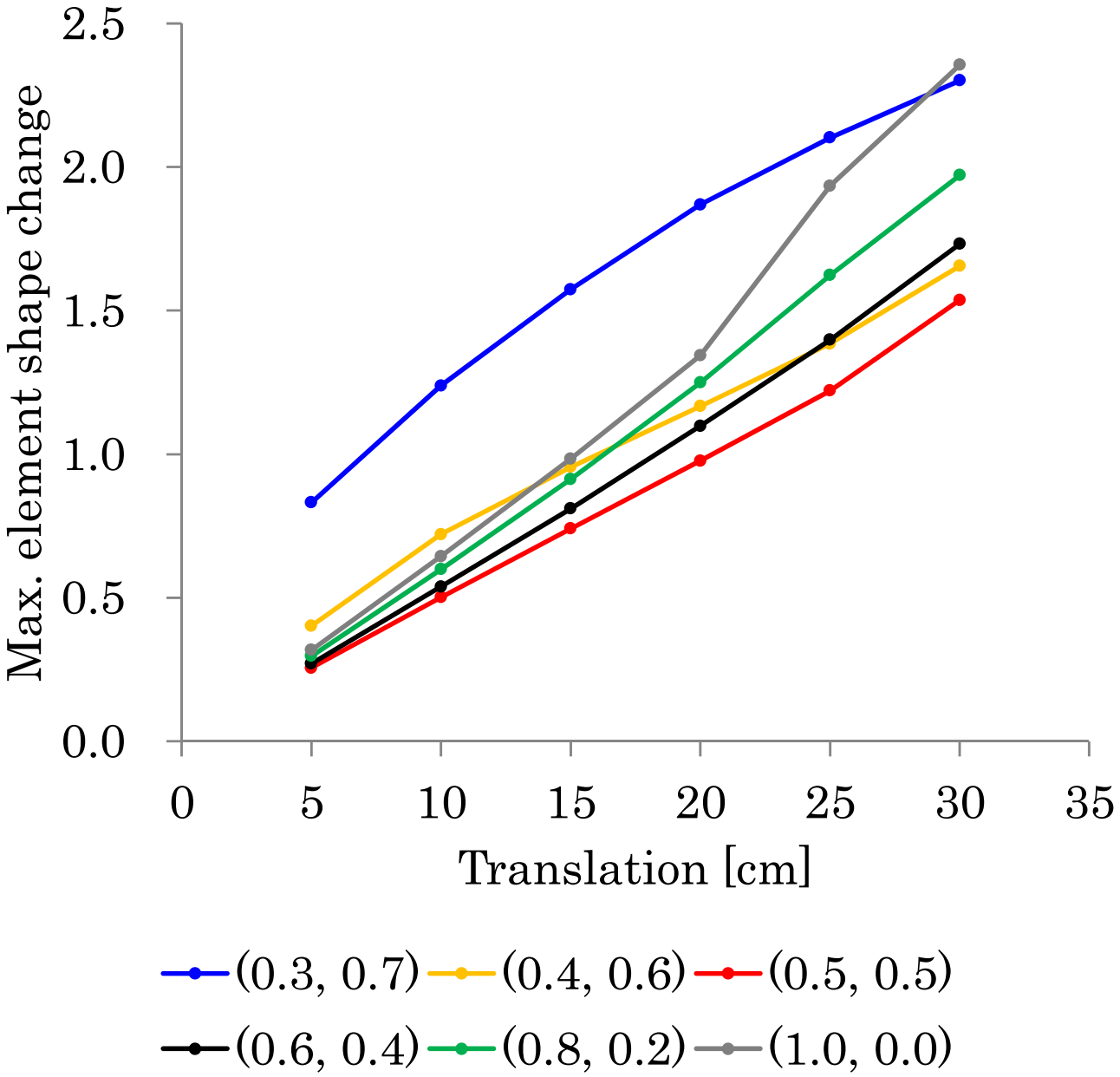

Figure 5 Maximum element shape change plotted against the translation of the structure for EQBS with different (χ_1, χ_2) values. (χ_1, χ_2) = (1.0, 0.0) and (0.5, 0.5) correspond to JBS and MHBS, respectively.

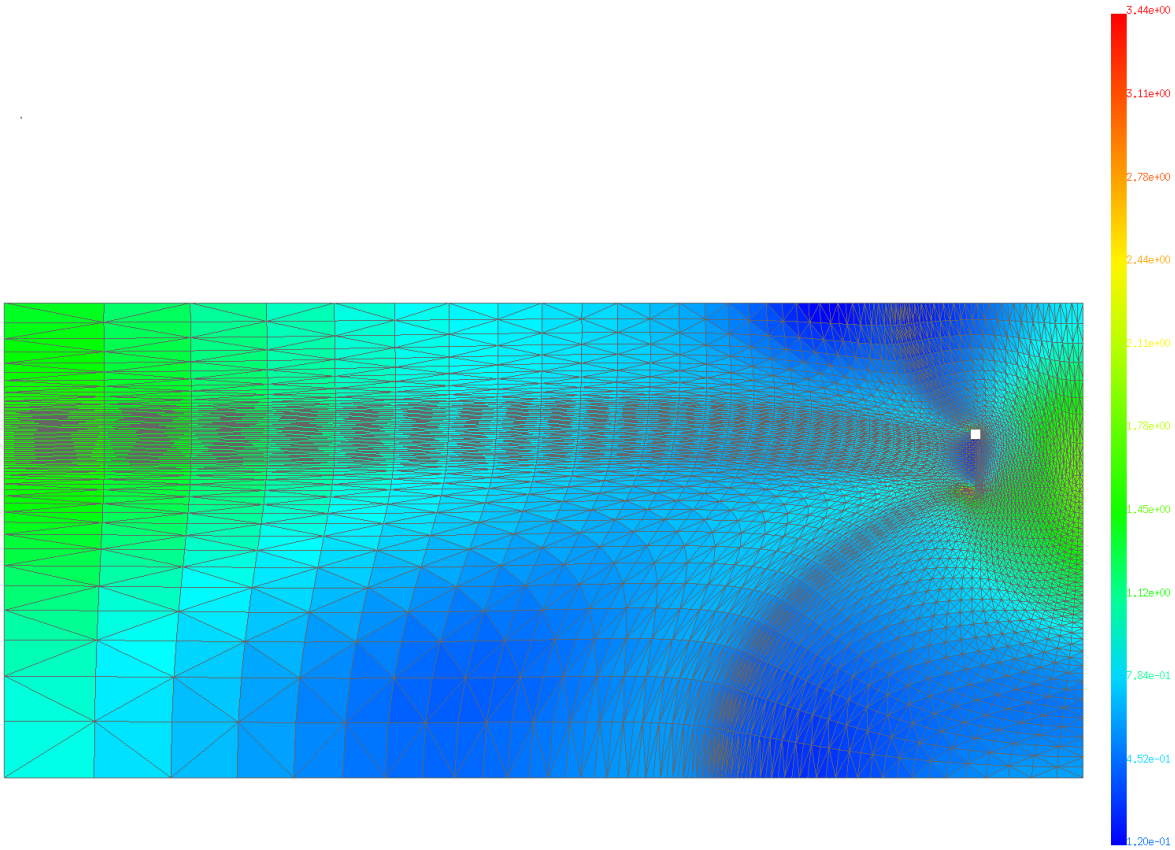

(a) $(\chi_1, \chi_2) = (1.0, 0.0)$ or JBS

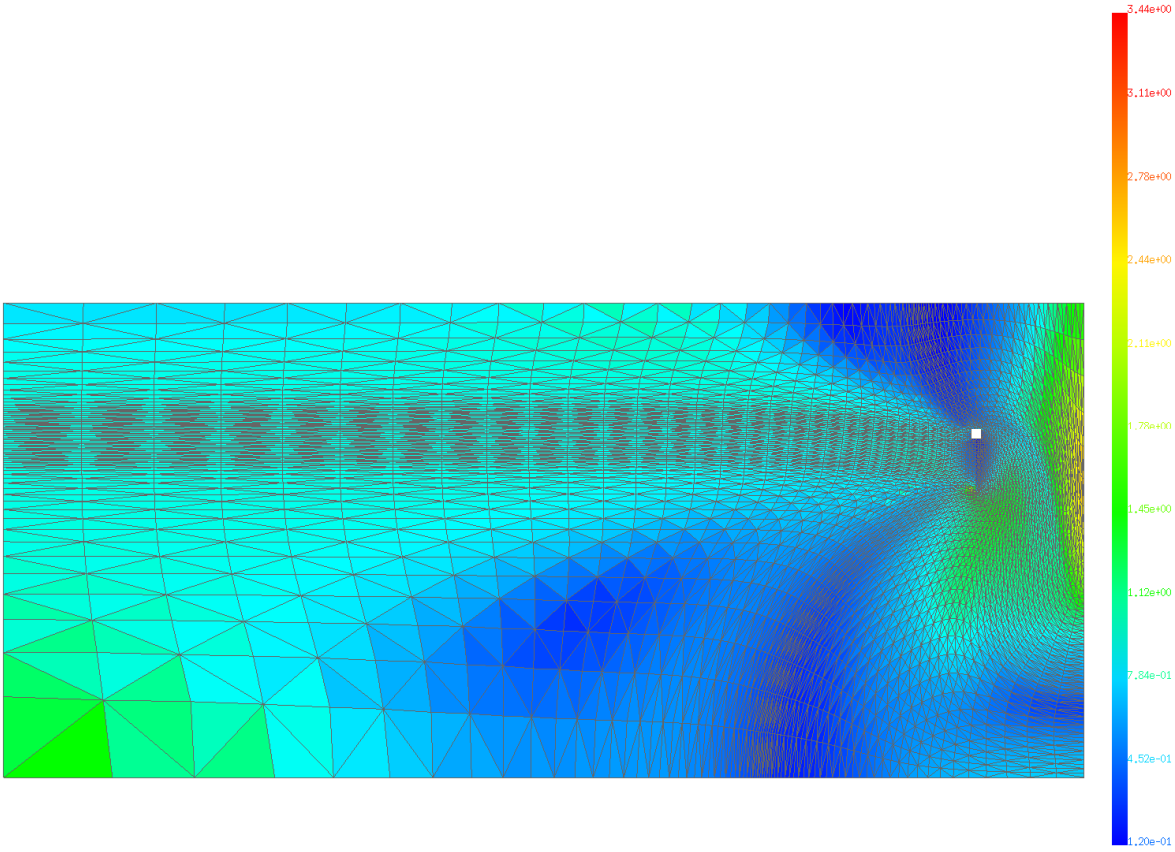

(b) $(\chi_1, \chi_2) = (0.5, 0.5)$ or MHBS

Figure 6 Equivalent strain distribution in the entire domain for $u_x^s = 30$cm.

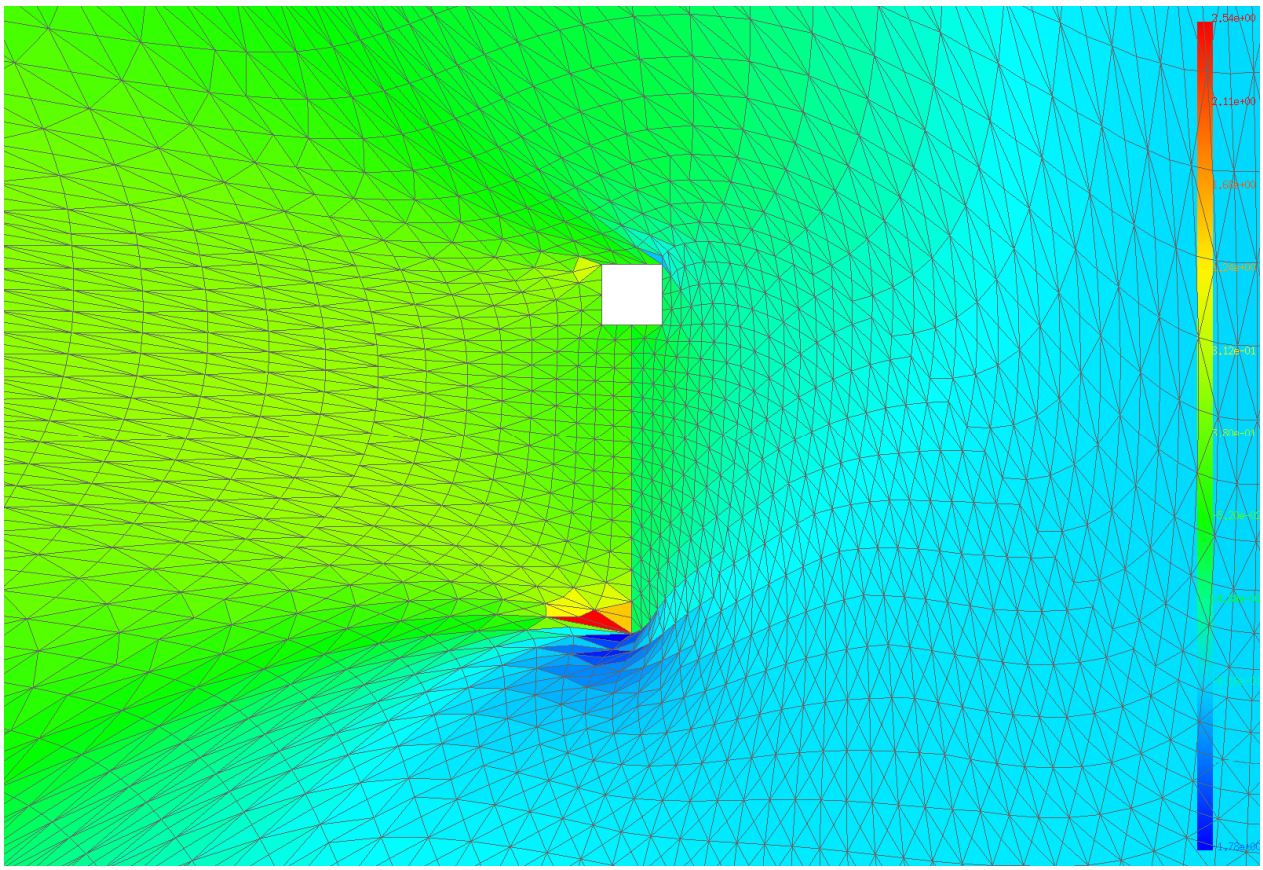

(a) (χ_1, χ_2) = (1.0, 0.0) or JBS

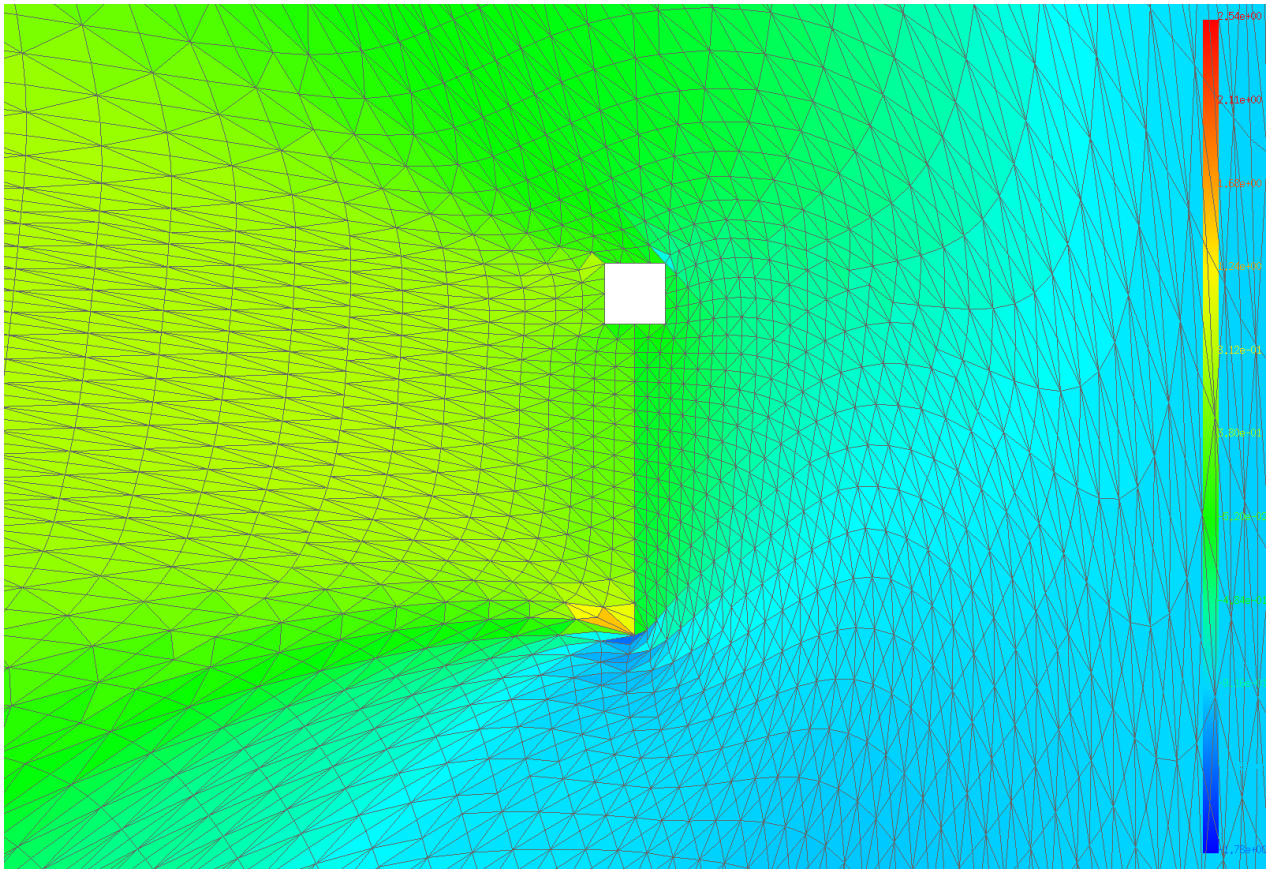

(b) (χ_1, χ_2) = (0.5, 0.5) or MHBS

Figure 7 Distribution of the tensile/compressive strain in the x-direction ε_{xx} near the structure for u_x^{s} = 30cm.

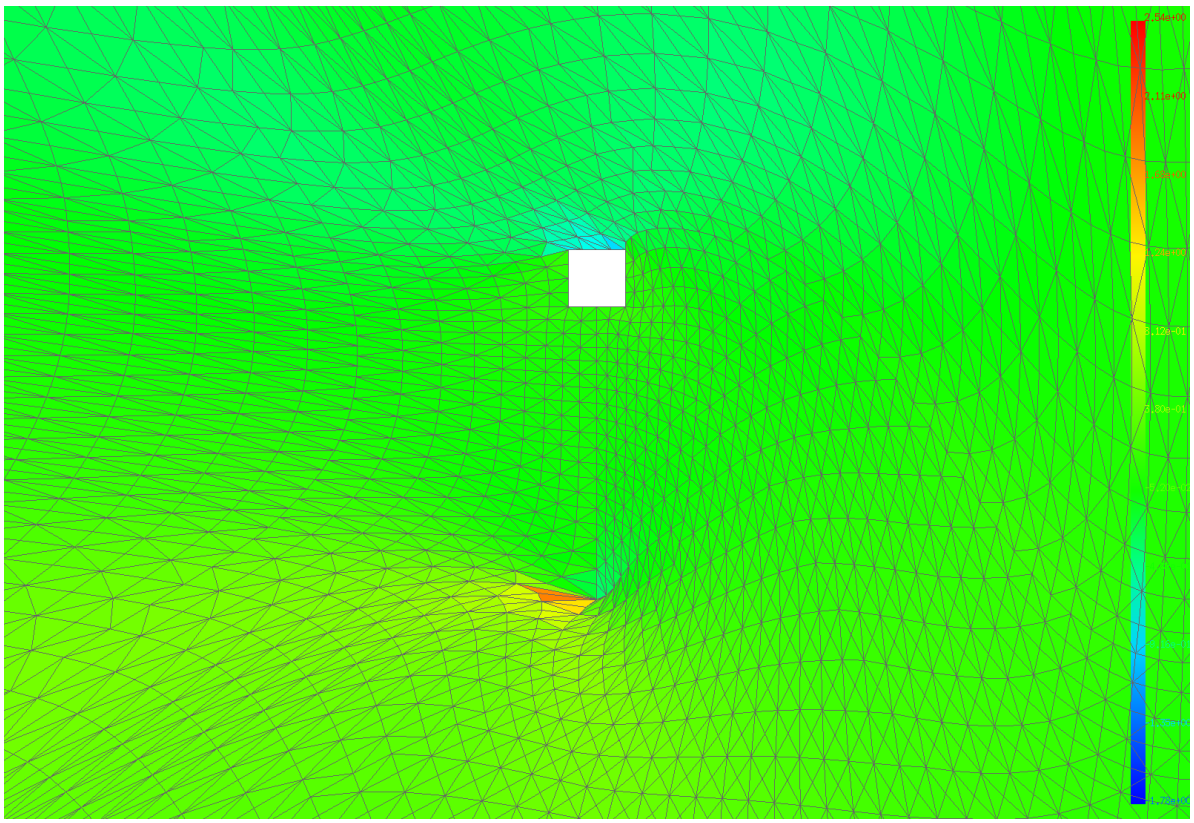

(a) $(\chi_1, \chi_2) = (1.0, 0.0)$ or JBS

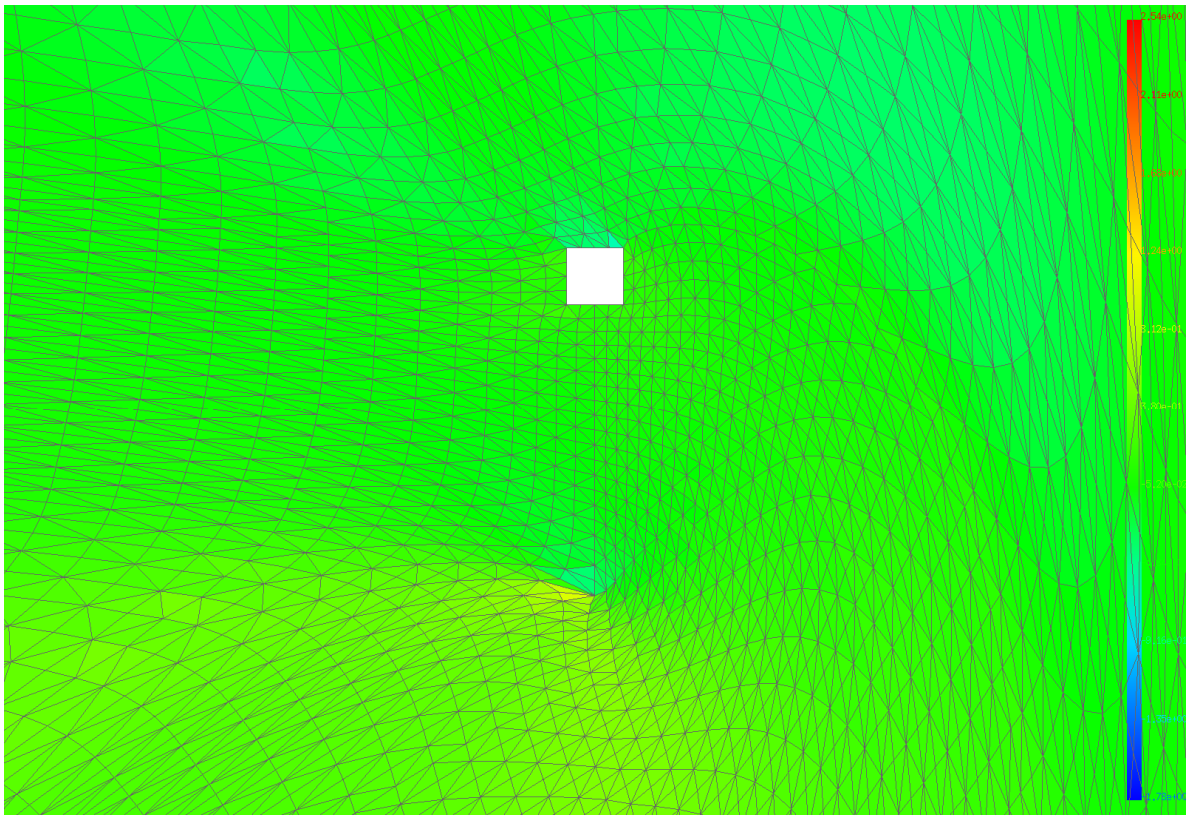

(b) $(\chi_1, \chi_2) = (0.5, 0.5)$ or MHBS

Figure 8 Distribution of the shear strain ε_{xy} near the structure for $u_x^{\,s} = 30$cm.

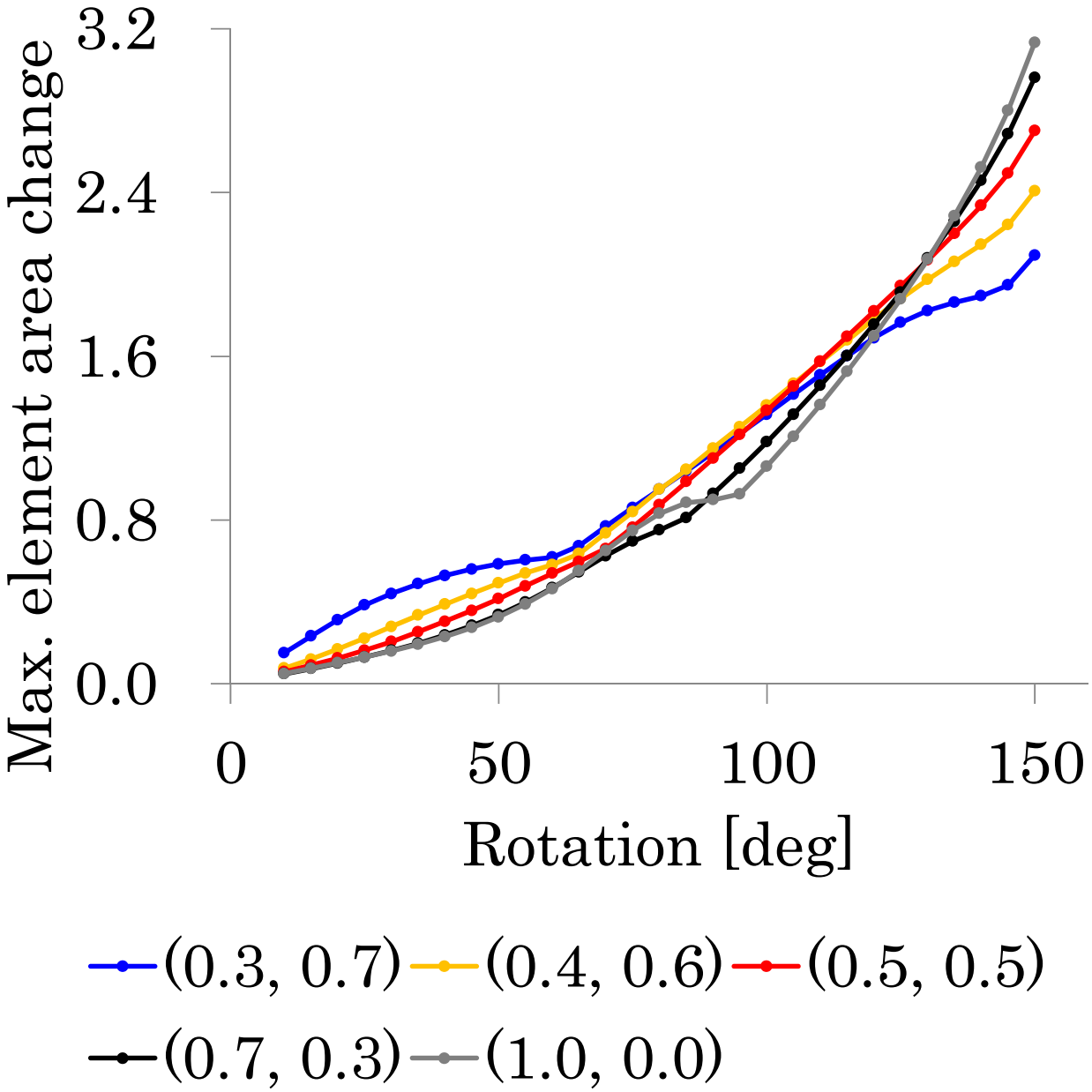

Figure 9 Maximum element area change plotted against structure rotations ranging from 10° to 150° for EQBS with different (χ_1, χ_2) values. (χ_1, χ_2) = (1.0, 0.0) and (0.5, 0.5) correspond to JBS and MHBS, respectively.

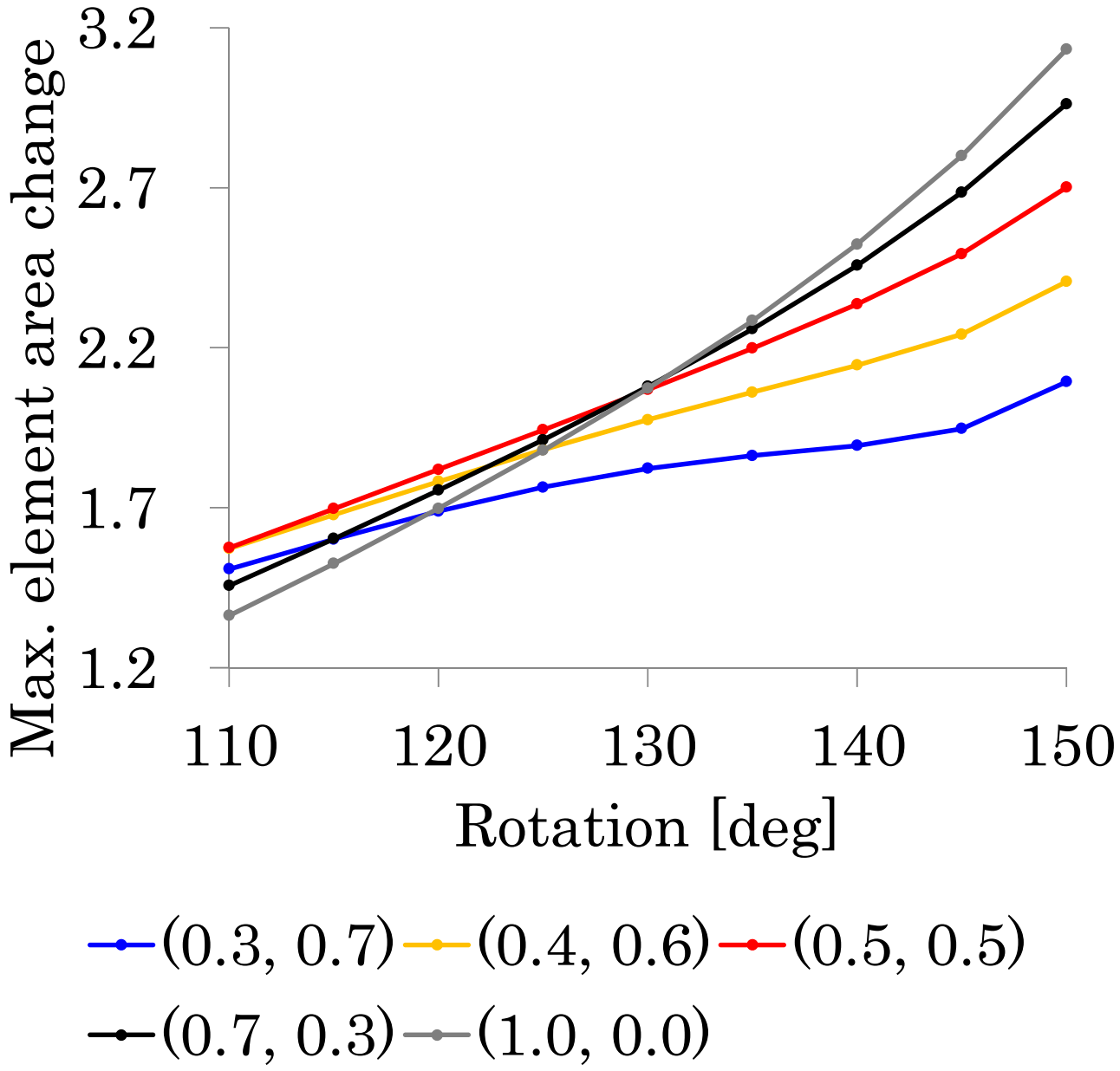

Figure 10 Maximum element area change plotted against structure rotations ranging from 110° to 150° for EQBS with different (χ_1, χ_2) values. (χ_1, χ_2) = (1.0, 0.0) and (0.5, 0.5) correspond to JBS and MHBS, respectively.

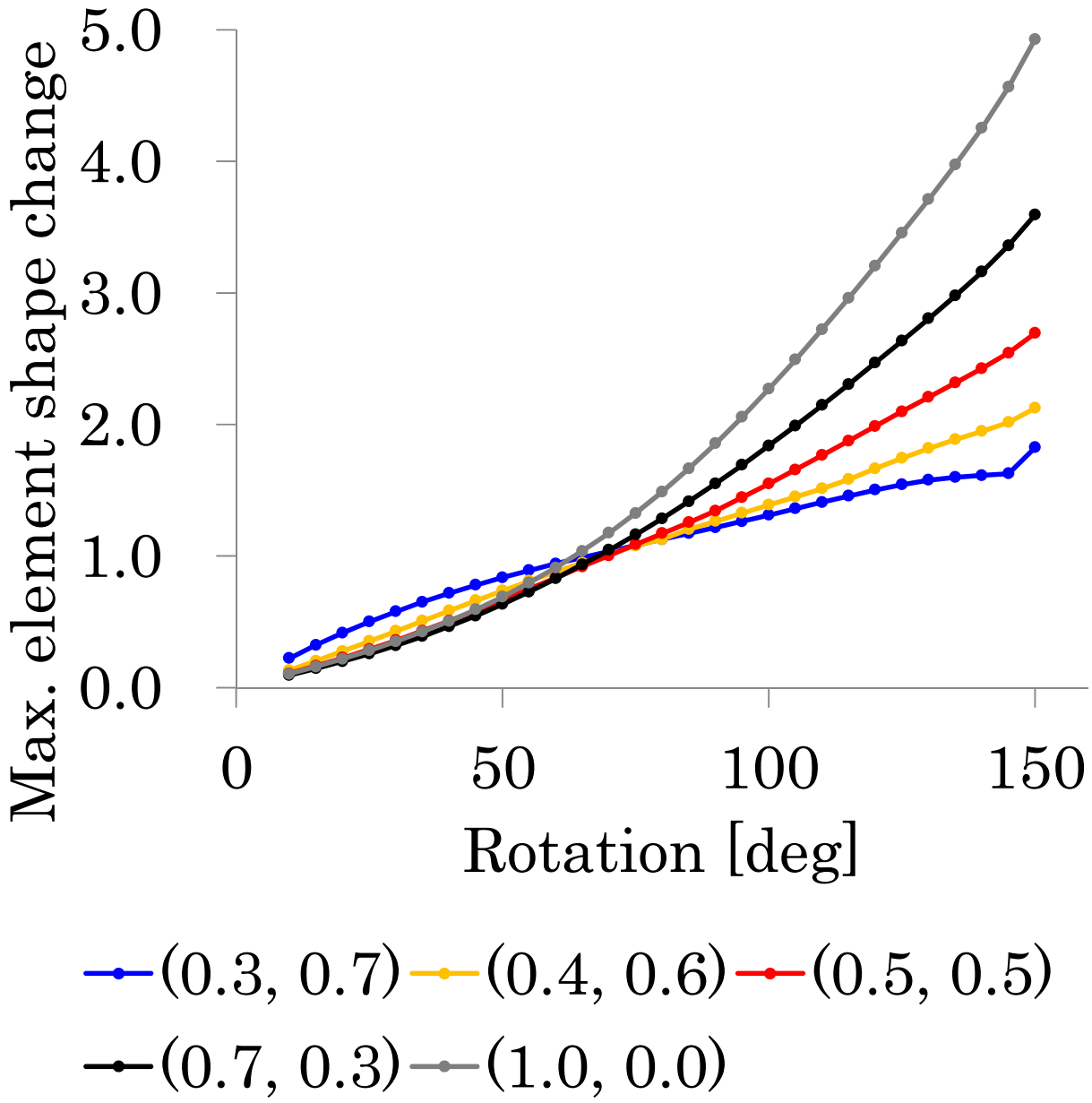

Figure 11 Maximum element shape change plotted against structure rotations ranging from 10° to 150° for EQBS with different (χ_1, χ_2) values. (χ_1, χ_2) = (1.0, 0.0) and (0.5, 0.5) correspond to JBS and MHBS, respectively.

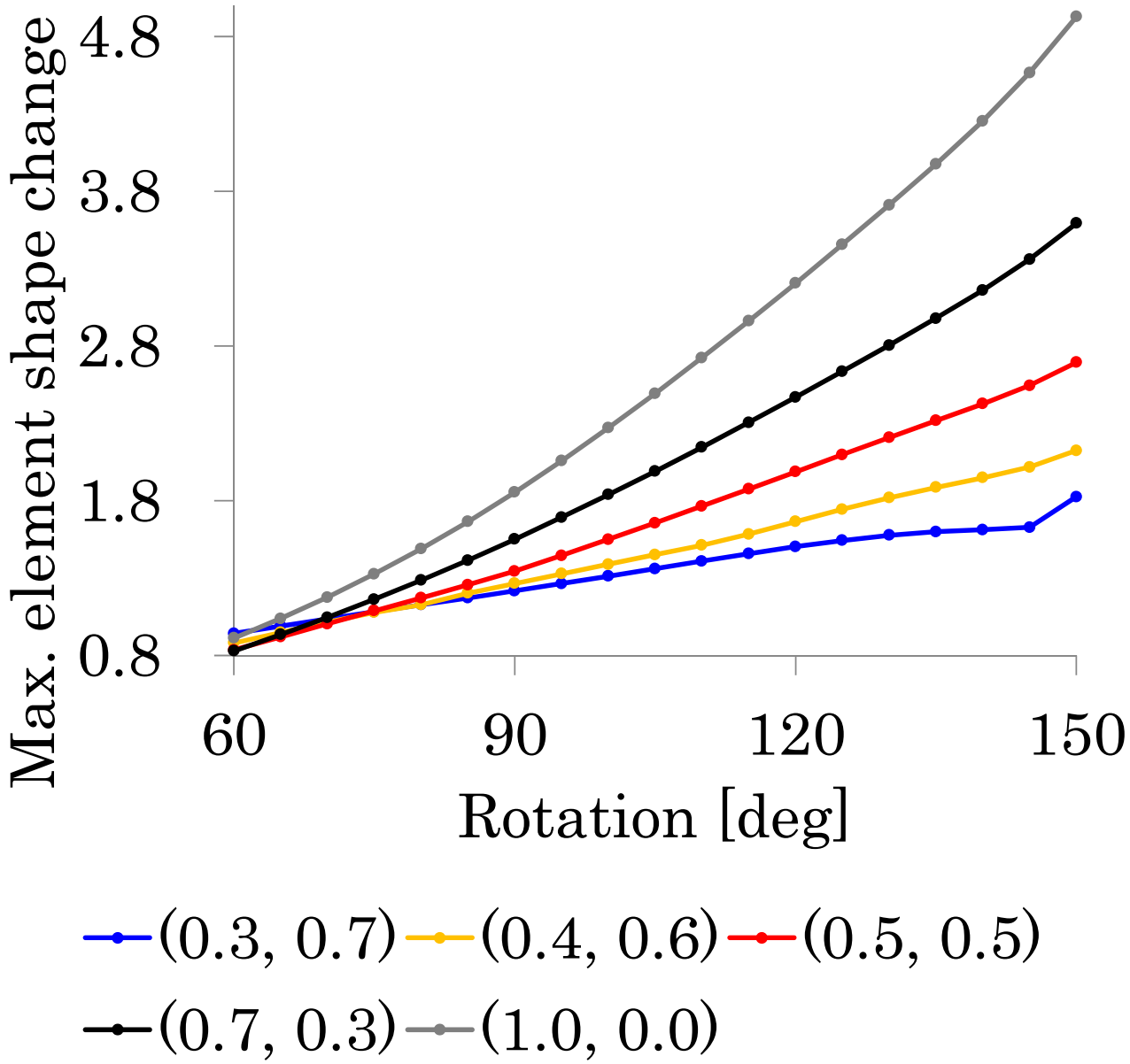

Figure 12 Maximum element shape change plotted against structure rotations ranging from 60° to 150° for EQBS with different (χ_1, χ_2) values. (χ_1, χ_2) = (1.0, 0.0) and (0.5, 0.5) correspond to JBS and MHBS, respectively.

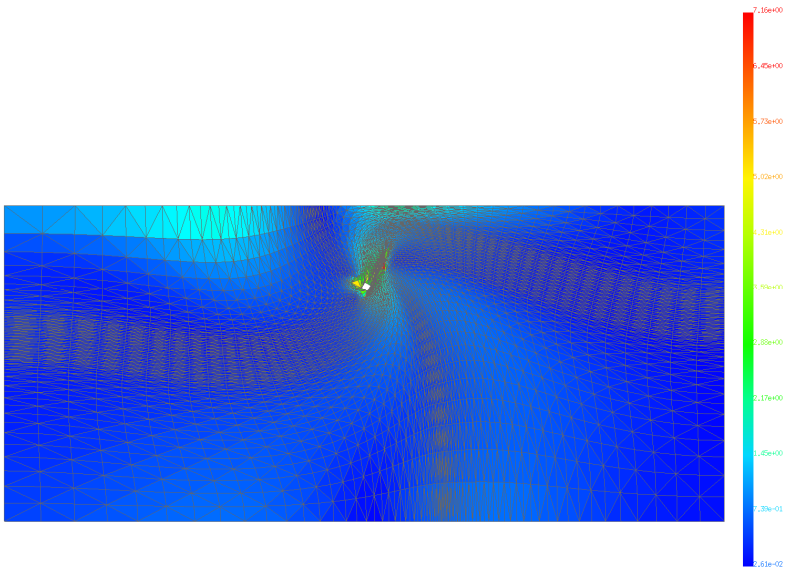

(a) (χ_1, χ_2) = (1.0, 0.0) or JBS

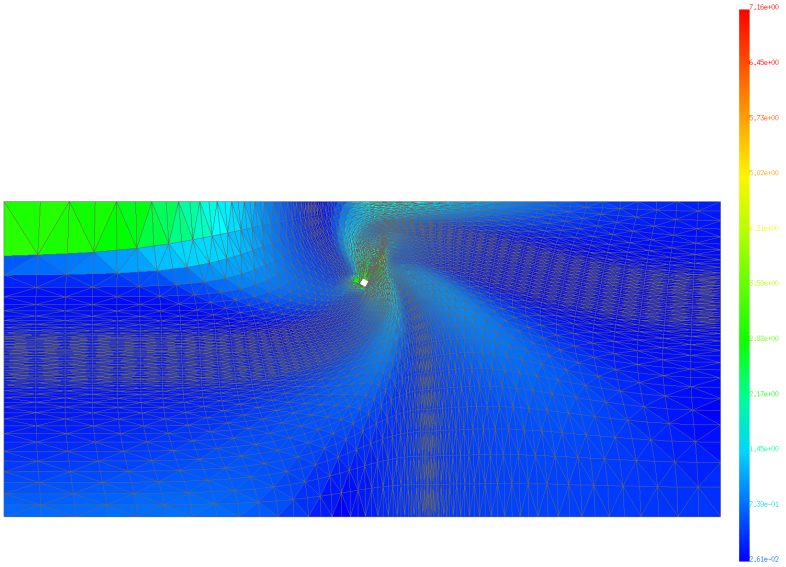

(b) (χ_1, χ_2) = (0.5, 0.5) or MHBS

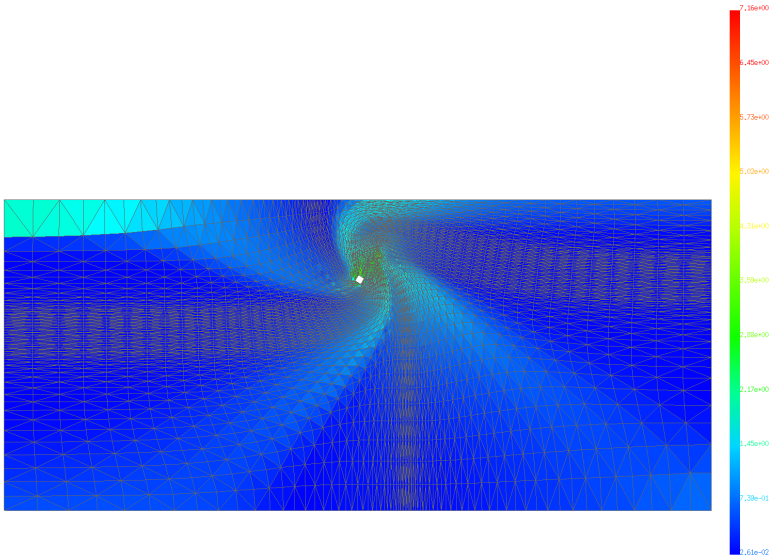

(c) (χ_1, χ_2) = (0.3, 0.7)

Figure 13 Equivalent strain distribution in the entire domain for θ^s = 150°.

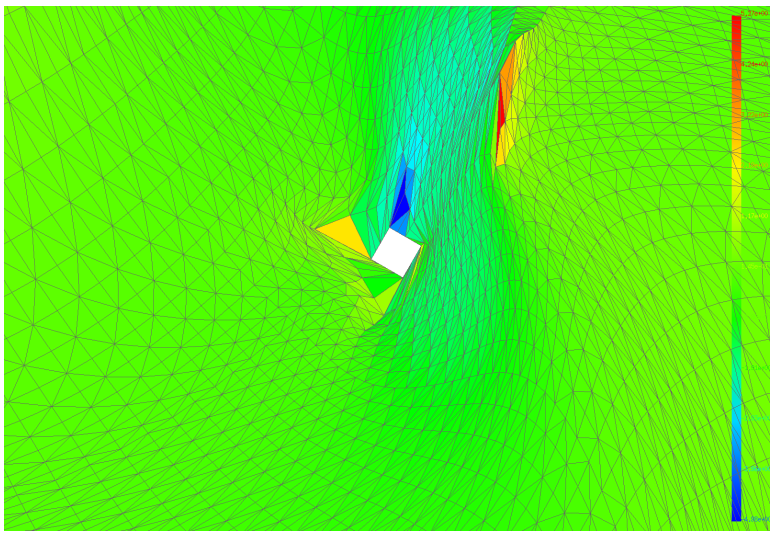

(a) $(\chi_1, \chi_2) = (1.0, 0.0)$ or JBS

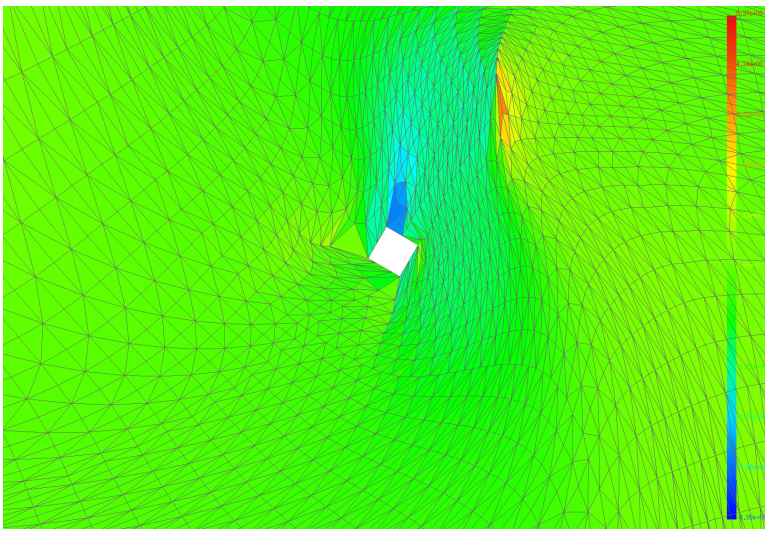

(b) $(\chi_1, \chi_2) = (0.5, 0.5)$ or MHBS

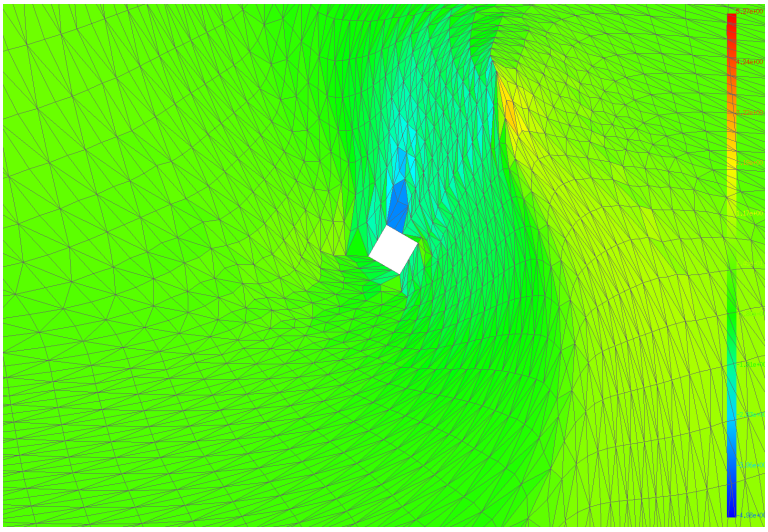

(c) $(\chi_1, \chi_2) = (0.3, 0.7)$

Figure 14 Distribution of the tensile/compressive strain in the y-direction ε_{yy} near the structure for $\theta^s = 150°$.

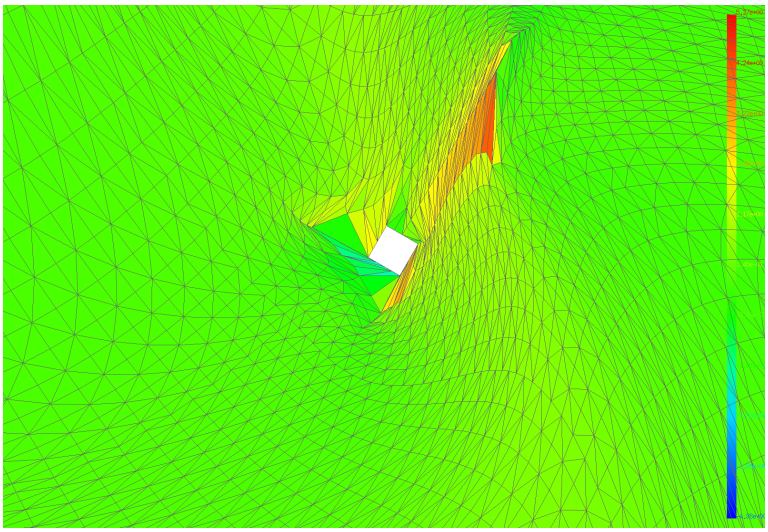

(a) $(\chi_1, \chi_2) = (1.0, 0.0)$ or JBS

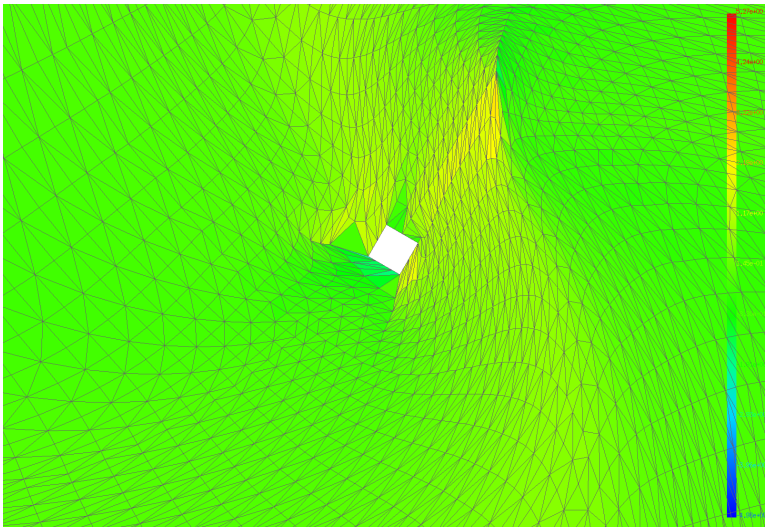

(b) $(\chi_1, \chi_2) = (0.5, 0.5)$ or MHBS

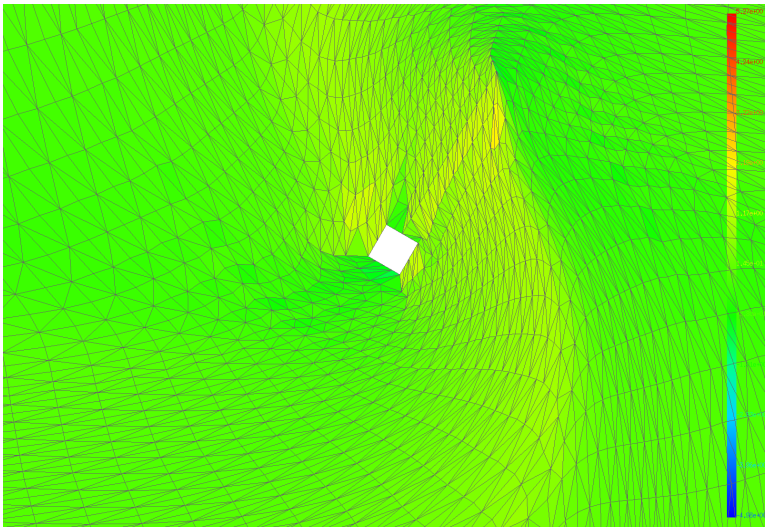

(c) $(\chi_1, \chi_2) = (0.3, 0.7)$

Figure 15 Distribution of the shear strain ε_{xy} near the structure for $\theta^s = 150°$.

TABLES

Table 1. Considered sets of χ_1, χ_2, and χ_3 values for the translation case.

χ_1	0.3	0.4	0.5	0.6	0.8	1.0
χ_2	0.7	0.6	0.5	0.4	0.2	0.0
χ_3	4.4	4.7	2.8	1.8	1.0	0.8
			(MHBS)			(JBS)

Table 2. Considered sets of χ_1, χ_2, and χ_3 values for the rotation case.

χ_1	0.3	0.4	0.5	0.7	1.0
χ_2	0.7	0.6	0.5	0.3	0.0
χ_3	6.2	4.5	3.4	2.3	1.5
			(MHBS)		(JBS)